Key Points:
- Increasing dynamic pressure increases polar cap potential during high driving
- Combination of models/mechanisms is needed to explain polar cap saturation
- Solar wind velocity increases the coupling efficiency between solar wind and polar cap

Interplay of solar wind parameters and physical mechanisms producing the saturation of the cross polar cap potential

M. Myllys[1] , E. K. J. Kipua[1], and B. Lavraud[2,3]

[1]Department of Physics, University of Helsinki, Helsinki, Finland, [2]Institut de Recherche en Astrophysique et Planétologie, Toulouse, France, [3]Centre National de la Recherche Scientifique, UMR 5277, Toulouse, France

Abstract The nonlinear response of the cross polar cap potential (CPCP) to solar wind driving electric field is a well-known phenomenon. The reasons behind this saturation, however, are still under debate. We have performed a statistical study of the coupling efficiency between the solar wind and the northern polar cap index (PCN). PCN is used as a proxy for the CPCP. Our main focus is in quantifying how the solar wind dynamic pressure alters the efficiency. We show that the saturation of PCN occurs both during low and moderate upstream M_A conditions. We also show that the increasing dynamic pressure is associated with increasing PCN. In addition, we find that the coupling is different depending on which parameter, the velocity or the magnetic field, increases the solar wind driving electric field: the higher the velocity the higher the coupling efficiency.

1. Introduction

Disturbances in the near-Earth environment are largely controlled by the highly variable solar wind. While magnetic reconnection at the dayside magnetopause has been established as the key mechanism allowing the transfer of energy, plasma, and momentum from the solar wind to the magnetosphere, the details of this interaction are still far from understood. One of the controversial topics related to the solar wind-magnetosphere coupling is the dependence of the cross polar cap potential (CPCP) on the upstream solar wind conditions [*Ridley*, 2005; *Lavraud and Borovsky*, 2008; *Kivelson and Ridley*, 2008; *Lopez et al.*, 2010; *Wilder et al.*, 2011].

In a simplistic view, the CPCP depends linearly on the solar wind dawn-dusk driving electric field ($E_{Y,SW}$) upstream of the bow shock. This is because the reconnection potential that maps into the high-latitude ionosphere along the equipotential field lines through the dayside reconnection line is in first approximation linearly correlated with the $E_{Y,SW}$. However, several studies have revealed nonlinearity (i.e., saturation) between the upstream driving electric field and CPCP, both using MHD simulations [*Siscoe et al.*, 2002a, 2002b; *Lavraud and Borovsky*, 2008; *Lopez et al.*, 2010] and observational data [*Reiff et al.*, 1981; *Reiff and Luhmann*, 1986; *Weimer et al.*, 1990; *Russell et al.*, 2001; *Ridley*, 2005; *Shepherd*, 2007; *Wilder et al.*, 2011; *Myllys et al.*, 2006].

Several models have been presented in the literature to explain the CPCP saturation (see the Appendix of *Borovsky et al.* [2009]). Some of the models predict that the CPCP saturates when the Alfven Mach number (M_A) in the solar wind is low [*Ridley*, 2007; *Kivelson and Ridley*, 2008; *Lavraud and Borovsky*, 2008; *Lopez et al.*, 2010; *Wilder et al.*, 2015]. *Lavraud and Borovsky* [2008] found that the plasma beta in the magnetosheath becomes small (even less than 1) during times of low M_A in the upstream solar wind and noted that the magnetic forces are enhanced. The main forces affecting the plasma flow in the magnetosheath are the $\mathbf{J} \times \mathbf{B}$ force and the plasma pressure gradient. During typical (high plasma beta) conditions the pressure gradient dominates but when the plasma beta becomes smaller the relative importance of the $\mathbf{J} \times \mathbf{B}$ force increases. Due to the changes in the force balance during low M_A conditions, the magnetosheath plasma streamlines are more diverted around the magnetopause which leads to the saturation according to *Lavraud and Borovsky* [2008]. Similar conclusions were reached by *Lopez et al.* [2010] who used MHD simulations to study the effect of the magnetosheath flow pattern for CPCP.

There are also models that highlight the effect of the Region 1 (R1) current system to the saturation. One of these models is called the Siscoe-Hill model. The first formulation of the model was based on the idea that the enhanced R1 currents induce a magnetic field that opposes the magnetospheric magnetic field, decreasing

the magnetic field on the magnetopause. This in turn lower the local Alfven speed leading to lower reconnection rates. Later, the model was improved by taking into account the fact that the pressure balance at the magnetopause is set by the force balance with the solar wind ram pressure. Thus, *Siscoe et al.* [2002b] suggested that the reason for the saturation lies in the limited R1 current system and not in the lowered reconnection rate. In this scenario, called as ram pressure model by *Siscoe et al.* [2002b], the dynamic pressure controls the upper limit of the R1 current.

Some of the CPCP saturation models are in contradiction with each other. For example, there is no agreement on the role of the solar wind dynamic pressure to the saturation process. There are models which assume that the saturation is caused by the shrinkage of the magnetosphere due to high dynamic pressure which shortens the reconnection X line length [*Raeder and Lu*, 2005; *Ridley*, 2005]. However, the ram pressure-saturation model by *Siscoe et al.* [2002b] predicts that during high solar wind driving, higher dynamic pressure leads to higher CPCP. Thus, the dynamic pressure is one parameter that can be used to distinguish between the models.

In this paper, we have performed statistical study of the coupling efficiency between solar wind and northern polar cap index (PCN). The coupling efficiency, which is defined as the ratio between the PCN index and the reconnection electric field, is studied under different M_A conditions, and the main focus is in finding how the solar wind dynamic pressure alters the efficiency. Since the dynamic pressure is a combination of mass density and plasma velocity, we also study the effect of velocity and density separately.

2. Data and Approach

The saturation of the CPCP during low Alfven Mach number (<3) conditions is well documented [*Ridley*, 2005; *Lavraud and Borovsky*, 2008; *Lopez et al.*, 2010; *Wilder et al.*, 2011; *Myllys et al.*, 2006]. However, *Myllys et al.* [2006] studied 80 interplanetary coronal mass ejection (ICME)-driven storms and noticed that CPCP saturates even during higher M_A (>7.2) conditions, suggesting that the saturation is not purely related to low M_A effects. In this study we use the whole OMNI data set from 1986 to 2015. *Myllys et al.* [2006] used the dawn-dusk interplanetary electric field component ($E_{Y,SW}$, GSM coordinates) as an estimate of the reconnection electric field and the northern polar cap index (PCN) as a proxy for the CPCP [e.g., *Troshichev et al.*, 1996; *Ridley and Kihn*, 2004]. We also adopt the PCN as proxy for the CPCP, but we use an expression for the reconnection electric field introduced by *Kan and Lee* [1979]. The formula is $E_R = V B_T \sin^2(\frac{\theta}{2})$, where V is the upstream plasma flow speed, B_T is the transverse magnitude of the interplanetary magnetic field (IMF) ($\sqrt{B_Y^2 + B_Z^2}$), and θ is the IMF clock angle ($\cos^{-1}(\frac{B_Z}{B_T})$). When the IMF is purely southward, E_R equals the magnitude of the interplanetary electric field.

The data used in this study are obtained through the near-Earth heliospheric database (OMNI, http://omniweb.gsfc.nasa.gov/) with 1 min resolution. OMNI data are composed of solar wind measurements from several spacecraft in geocentric or Lagrangian L1 orbits (at the time of this study the data consist mainly of Wind and ACE measurements). The data are propagated to the nose of the Earth's bow shock. The IMF and electric field components we use here are in GSM coordinates. The PCN index is also downloaded from the OMNIWeb. To account the time delay between the solar wind and PCN measurements, we use time lag of 17 min and averaging time window of 27 min determined by *Myllys et al.* [2006]. We smooth the solar wind data because the magnetosphere is not sensitive to the smallest fluctuations in the solar wind parameters and it acts as a low-pass filter [*Clauer et al.*, 1981; *Takalo et al.*, 2000; *Ilie et al.*, 2010]. By smoothing the solar wind data we maximize the correlation between the solar wind and the PCN measurements.

Since the aim of the paper is to compare some of the existing saturation models with observations, we divide first our data set into two groups based on the M_A values. The first M_A group includes data points when M_A is below 5, and the second group when M_A is higher than 5. The limiting value 5 was selected based on the assumption that low M_A mechanisms like the magnetosheath flow diversion due to increased magnetic forces in the magnetosheath cannot act when M_A is sufficiently high (>5) [*Lavraud and Borovsky*, 2008; *Lopez et al.*, 2010]. Thus, we should not see the saturation of PCN when we study the high M_A group if the saturation depends only on effect related to low M_A. However, as we will demonstrate, this is not the case.

Figure 1 shows the PCN as a function of E_R for the OMNI measurements between 1986 and 2015. Different curves represent different M_A groups described above. For both M_A groups the measurements were binned according to the E_R value. The width of the E_R bin is 0.5 mV/m, and the E_R range is from 0 to 40 mV/m.
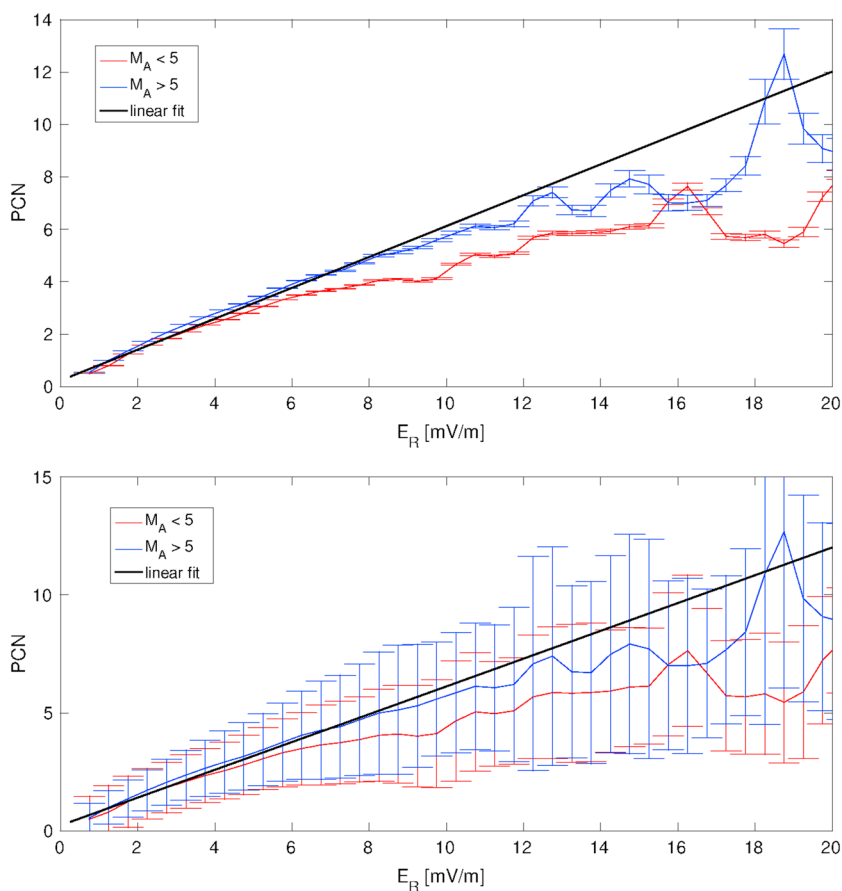
Figure 1. PCN as a function of E_R for two different M_A levels. The red curve is showing the times when M_A is lower than 5 and the blue curve when M_A is higher than 5. The error bars show the (top) standard error of the mean and the (bottom) standard deviation. The black line is linear fit to the linear part of the curves ($E_R < 5$), and it represents linear dependence between PCN and E_R.

The mean value of the PCN was computed inside each E_R bin (see Figure S1 in the supporting information for PCN medians). In Figure 1 the red (blue) curve includes observations when $M_A < 5$ ($M_A > 5$). The error bars in Figure 1 (top) show the standard error of the mean (SEM), and in Figure 1 (bottom) they represent the standard deviation (SD) of the data. The SEM is the standard deviation of mean of random samples of the measured quantity, and it is a measure for the uncertainty in the estimate of the mean. The definition for the SEM is $\sigma = \frac{SD}{\sqrt{n}}$ where SD is the standard deviation of the sample and n is the sample size. There are E_R measurements up to 40 mV/m, but the data coverage is very limited above 20 mV/m so the E_R axes are limited from 0 to 20 mV/m.

The black line in Figure 1 represents the linear dependence between PCN and E_R. It is added to highlight the nonlinearity of the two different M_A curves. As can be seen from Figure 1, red curve starts to show some nonlinearity after E_R exceeds 3 mV/m and blue curve when E_R is above 6 mV/m. The low M_A curve (red) flattens faster than the high M_A curve (blue). This indicates that the effects related to low M_A amplify the saturation, but the saturation is not related solely to the upstream M_A conditions (or magnetosheath plasma beta). Figure 1 confirms the previous finding by *Myllys et al.* [2006] that the saturation can happen even during higher M_A conditions. We also note that the low M_A curve has a lower scatter than the high M_A curve (Figure 1, bottom). This is partly due the fact that the M_A range is wider for the blue curve than for the red.

In the following sections, we use the same two M_A groups as in Figure 1. Since the standard error of the mean (Figure 1, top) starts to increase after E_R is greater than 12 mV/m especially for the high M_A group due to increasing scatter of the data (Figure 1, bottom) and decreasing number of data points (not shown), we study E_R range from 0 to 12 mV/m.
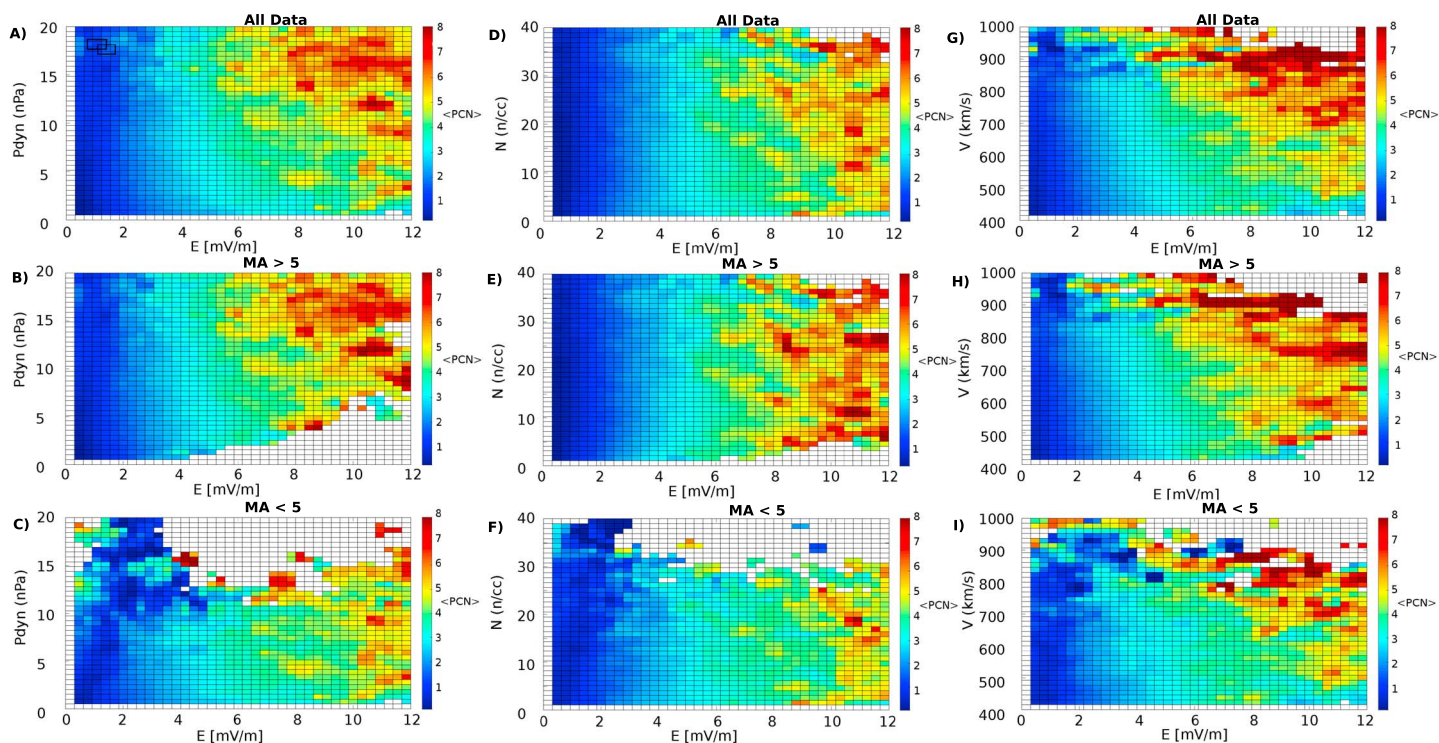
Figure 2. (a–c) Dynamic pressure (p_{dyn}), (d–f), density (N), and (g–i) velocity (V) as a function of E_R. The color of the bin shows average PCN value inside the bin.

3. Results

3.1. PCN Dependence on Solar Wind Parameters

To study how PCN is affected by the upstream dynamic pressure (P_{dyn}) during different E_R conditions, data points were divided into 0.5 nPa × 0.3 mV/m bins based on the P_{dyn} and E_R values and the mean PCN value inside each bin was computed. To smooth the statistics, the bin size was increased by taking observations from the bin center to 0.15 mV/m in E_R direction and to 0.25 nPa in P_{dyn}. Thus, the resulting bin size is 1 nPa × 0.6 mV/m, and the bins are partly overlapping. The results are shown in Figures 2a–2c. The overlapping bin is visualized in Figure 2a using a black bolded square. At least 10 measurement points were required for each extended bin when the PCN averages were computed. The maps showing the number of data points in each extended bins can be found in the supporting information (Figure S2).

Figure 2a includes all 1 min data points during 1986–2015, while Figures 2b and 2c are organized based on the M_A conditions using the same limiting value $M_A = 5$ as in Figure 1. This allows us to study separately the times when the saturation mechanism related to low solar wind M_A (i.e., low magnetosheath plasma beta) conditions is likely to occur and the times when low M_A effects can be ignored.

Figure 2 shows how the P_{dyn} affects the mean PCN value during different E_R periods. When solar wind driving is weak ($E_R = 0-3$ mV/m), the pressure has almost negligible effect (i.e., PCN stays between 0 and 2.5). However, when E_R increases above 3 mV/m, we find that PCN slowly increases with increasing P_{dyn}. During the most intense driving periods ($E_R = 8$ 12 mV/m) PCN is clearly depended on the P_{dyn} value. The highest PCN values (7–8) are achieved only when both P_{dyn} and E_R are high.

When P_{dyn} and E_R dependence is studied during high M_A (>5) conditions (Figure 2b), the PCN has similar pattern in the case of all data. The most notable difference is that there are no small P_{dyn} values when solar wind driving is moderate to intense ($E_R = 5-12$ mV/m). Since the high M_A group has more data points compared to low M_A group (See Figure S1 in the supporting information), the high M_A times have higher contribution to the All Data map (Figure 2a). In the case of small M_A the highest P_{dyn} values (12–20 nPa) are missing almost through the whole E_R range except a few values during weak driving. The gradient of PCN is still visible for small M_A when E_R range is from 4 to 10 mV/m.
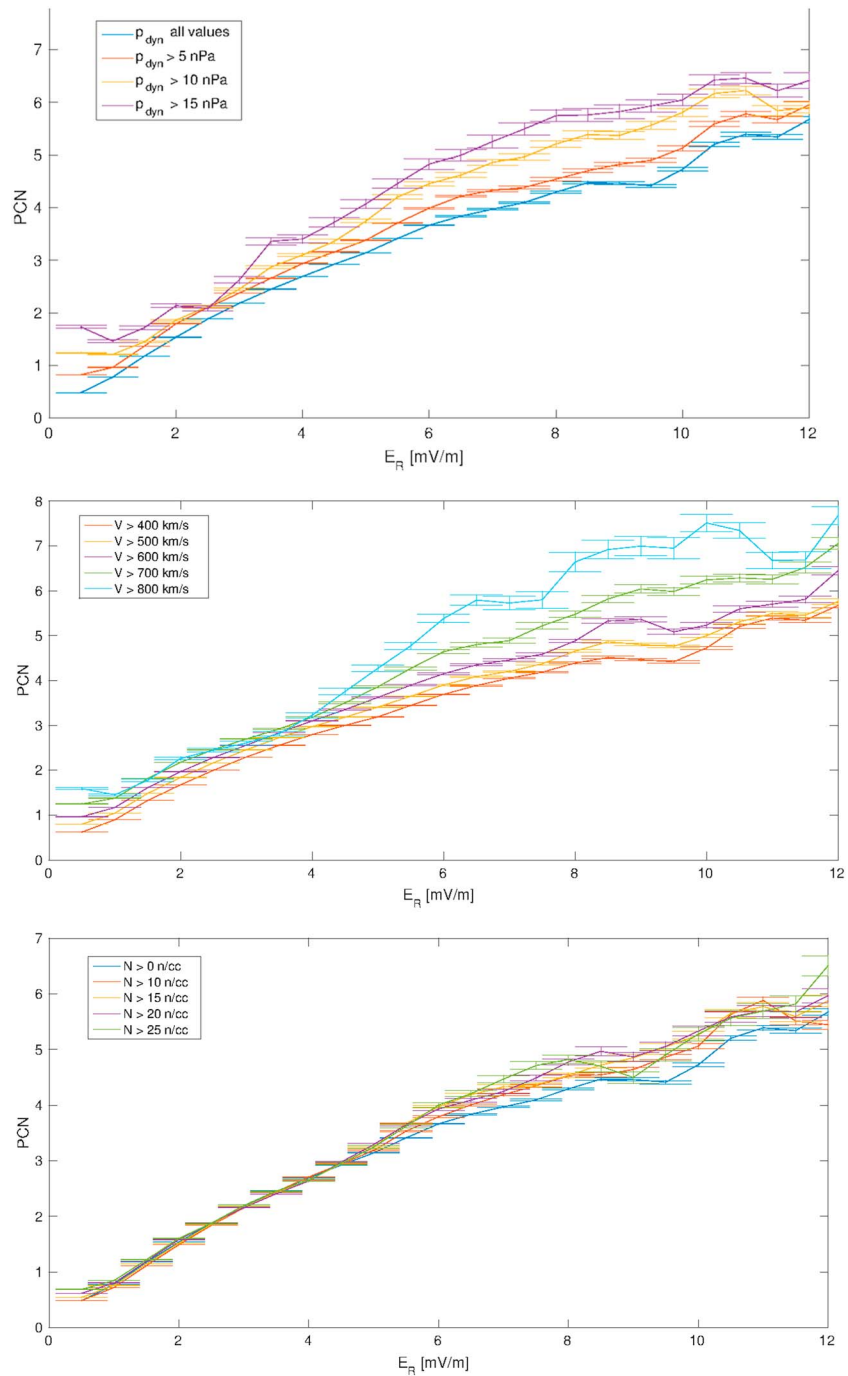
Figure 3. PCN as function of E_R during different (top) P_{dyn}, (middle) V, and (bottom) N levels. The error bars show the standard error of the mean.

Because the dynamic pressure ($P_{dyn} = \rho V^2$) is defined using the plasma flow speed (V) and mass density (ρ), the plasma velocity and number density (N) are also plotted as function of E_R (see Figures 2d–2i). In the case of density, the data were divided into 1 n/cc × 0.3 mV/m bins. For the velocity the bin size is 15.4 km/s × 0.3 mV/m. For the density and velocity plots the bin size was increased as it was for P_{dyn}.

The PCN show very weak dependence on density. For high M_A conditions (Figure 2e) the density dependence is almost completely missing. For all data points and low M_A maps (Figures 2d and 2f) there is a weak dependence when E_R is between 5 and 10 mV/m. In the case of low M_A this can be partly caused by the fact that the

higher density typically means also higher M_A, and thus, the highest density values correspond to the highest M_As (near 5) in Figure 2f. This weakens the low M_A effects in the magnetosheath and can lead to a higher coupling efficiency.

When the effects of P_{dyn}, N, and V are compared as a function of E_R, the velocity seems to affect to PCN the most. The following feature is true for the whole E_R range and for all M_A conditions: the higher the velocity, the higher the PCN (Figures 2g – 2i). The PCN color gradient starts to be visible already when E_R is around 2 mV/m. If the high and low M_A groups are compared, it is clear that PCN grows more slowly during low M_A. The reason for this can be seen in Figure 1. PCN is always lower for low M_A compared to high M_A. Figure 2g demonstrates that it does matter whether E_R is increased by the magnetic field or by the velocity (see also Figures S3 and S4 in the supporting information). The coupling efficiency, when measured using PCN, is increased when E_R is intensified due to high velocity.

Figure 3 shows PCN as a function of E_R. In Figure 3 (top), different colors represent different P_{dyn} levels. The blue curve (Figure 3, bottom) consists of all data points, the red curve includes data points when $P_{dyn} > 5$ nPa, yellow curve when $P_{dyn} > 10$ nPa, and the purple curve (Figure 3, top) when $P_{dyn} > 15$ nPa. The data have been averaged using regular E_R bins similar to the curves in Figure 1. The error bars show the standard error of the mean inside each E_R bins. Figure 3 shows the same feature as the color map in Figure 2a: the highest values for pressure correspond to highest PCNs. Figures 3 (middle and bottom) show similar curves for different V and N levels. The velocity has the same trend as P_{dyn}: the highest V values leads to the highest PCN values. In the case of density, there is no clear dependence on PCN for different N levels which is consistent with Figure 1d.

4. Meaning of the Results in Terms of Existing Saturation Models

In this paper, we have presented some observational features of CPCP, using PCN as a proxy, as a function of different solar wind parameters.

Our main results are the following.

1. PCN increases with increasing solar wind dynamic pressure during high solar wind electric field driving.
2. Increasing solar wind velocity increases PCN throughout the whole E_R range, but the velocity effect is most distinct during high E_R.
3. Density is not important to PCN except during low M_A conditions.
4. The PCN saturation is clearest during low M_A (<5) conditions with small scatter of the data, but it is also visible when M_A increases above 5.

These remarks combined with previously published observations can be used to distinguish between different saturation models. For example, the role of the dynamic pressure for CPCP has been unclear as discussed in section 1. Since the dynamic pressure affects the length of the reconnection X line at the magnetopause, the shortening of the X line has been proposed to be the cause or at least an important factor [*Raeder and Lu*, 2005; *Ridley*, 2005] for CPCP saturation. However, Result 1 above is in contradiction with the X line length model.

On the other hand, the Siscoe-Hill ram pressure model predicts that the CPCP is insensitive to P_{dyn} during weak solar wind driving but the dynamic pressure increases CPCP during intense driving. It is important to note that even though increasing P_{dyn} enhances CPCP, the ram pressure model also includes the so-called Chapman-Ferraro scaling [*Vasyliunas et al.*, 1982] which means the effect of the X line length shortening due to increasing P_{dyn} [*Siscoe et al.*, 2002a].

In the simplest form, Hill's formulation [*Hill et al.*, 1976] for the CPCP (Φ) can be expressed as a combination of the linearly increased potential (Φ_L) and the saturated value of the potential (Φ_S):

$$\Phi = \frac{\Phi_L}{1 + \frac{\Phi_L}{\Phi_S}} \tag{1}$$

According to equation 1, the saturation is defined by the term $\frac{\Phi_L}{\Phi_S}$. When the formulas for Φ_L and Φ_S given by *Siscoe et al.* [2002b] (equations (2) and (6) in the Siscoe's paper) are taken into account, it can be seen that the term $\frac{\Phi_L}{\Phi_S}$ is only related to the upstream Alfven speed and ionospheric conductivity. *Lavraud and Borovsky* [2008] call the term Q parameter (see their equation (7)), and they point out that this parameter is typically high when M_A is low. Thus, if the low M_A is due to high B and low N, which is typically the case during magnetic

clouds [*Lavraud and Borovsky*, 2008], the magnetosheath force balance model and the Siscoe-Hill model both predict the saturation. However, the Siscoe-Hill model does not depend on the magnetosheath beta and thus can saturate over wider range of upstream M_A conditions.

The dependence of PCN on P_{dyn} in the ram pressure model is more or less in agreement with our results. Nonetheless, the functional form of Φ_H (equation (6) in *Siscoe et al.* [2002b]) does not fully fit our observations (see Figure S5 in the supporting information). In addition, the fact that Q factor, which defines the saturation in the Siscoe-Hill model, depends on the Alfven speed is also problematic regarding our results; because the Alfven speed is related to the mass density according to the Siscoe-Hill model the CPCP saturation should have a clear dependence on density. As discussed above, our results show only very weak density dependence. In addition, the Siscoe-Hill model does not take into account the strong V dependence of coupling efficiency either.

The Siscoe-Hill formula for the CPCP also depends on the ionospheric conductivity. We have, however, ignored the effect and just assume that it is one source of the scatter in the data. As our data set covers more than two solar cycles, we assume that the solar cycle effects to the ionospheric conductivity are averaged out.

5. Discussion

Recently, the saturation of the electric field and the Poynting flux in the Earth's magnetosheath has been suggested as the cause of the polar cap saturation. *Pulkkinen et al.* [2016] showed using the Time History of Events and Macroscale Interactions during Substorms observations in the magnetosheath combined with the OMNI solar wind data that the magnetosheath electric field and Poynting flux saturate during intense solar wind driving. This means that these quantities in the magnetosheath do not increase linearly with the solar wind parameters upstream of the bow shock. However, the directly driven part of the auroral electrojets was observed to correlate well with the normal component of the Poynting flux at the magnetopause. Thus, *Pulkkinen et al.* [2016] conclude that the polar cap saturation is primarily caused by the processes associated with the bow shock crossings and plasma motion in the magnetosheath. The saturation mechanism proposed by *Pulkkinen et al.* [2016] is interesting in terms of the magnetosheath force balance model because flow diversion due to increased magnetic forces in the magnetosheath [*Lavraud and Borovsky*, 2008; *Lopez et al.*, 2010] also predicts saturated electric field near the magnetopause.

The role of the magnetosheath properties to CPCP saturation was also highlighted by *Clauer et al.* [2016]. The authors studied the electric field near the throat of reverse ionospheric convection cells during an ICME event with extremely strong northward IMF and found no evidence of saturation of the ionospheric electric field. Because the upstream number density and velocity were high during the ICME ($V \approx 600$ km/s and $N \approx 20$ n/cc), the authors state that lack of saturation may be related to high magnetosheath plasma beta.

Figure 2a demonstrates that the dynamic pressure increases PCN during intense driving, which as discussed in the previous section contradicts with the X line length model [*Raeder and Lu*, 2005]. Previously, *Ober et al.* [2003] studied the prediction given by the Siscoe-Hill model using Defense Meteorological Satellite Program (DMSP) measurements of the polar cap potential and noted that the temporal variations in DMSP potential were in a good agreement with the predicted values. *Ober et al.* [2003] estimated ionospheric Pedersen conductivity using 10.7 cm solar radio flux and also compared the events with similar solar flux conditions but with different P_{dyn} conditions. The authors found that DMSP yielded higher potential when P_{dyn} was higher. Thus, the results by *Ober et al.* [2003] also show negative support to X line length model.

The saturation models that are in agreement with the results of this paper seem to highlight the role of magnetosheath and R1 currents to the saturation. For example, the magnetosheath force balance model depends on the magnetosheath properties, while the Siscoe-Hill model relies on the R1 currents. Thus, it seems that to explain the saturation both the magnetosheath dynamics and R1 currents should be taken into account.

Based on the results shown in this paper and previous literature, it seems that several mechanisms may contribute to the saturation and that different mechanisms dominate during different conditions. In addition, it is clear that none of the existing models can fully explain the saturation. For example, magnetosheath flow diversion (i.e., magnetosheath force balance) can explain the saturation during the lowest M_A times, supported by the results by *Pulkkinen et al.* [2016], but the flow diversion is unable to explain why saturation occurs even when M_A is above 5.

6. Conclusions

In this paper we have shown that the saturation of the PCN occurs both during low and moderate upstream M_A conditions. Our results also highlight the difficulties of the existing polar cap saturation models to explain the saturation during all solar wind conditions, and combination of models is needed to explain the details of saturation. We found that the solar wind coupling is different depending on which parameter, the velocity or the magnetic field, makes the solar wind driving electric field high; the higher the velocity the higher the coupling efficiency when determined by PCN. This is in agreement with *Pulkkinen et al.* [2015] who found that the energy transfer determined by the magnetosheath Poynting flux increases in particular when the solar wind speed is high. We have also shown statistically that the dynamic pressure increases the PCN value during intense solar wind driving. This is particularly interesting considering the generation of extreme space weather storms. Sheath regions of coronal mass ejections (CMEs) and also parts of interacting CMEs tend to have clearly larger dynamic pressure than the unperturbed CME flux rope [*Kilpua et al.*, 2013]. As a consequence, our results imply that CME sheaths and interacting CMEs are expected to be related to most efficient solar wind-magnetosphere coupling and strongest geospace disturbances.

References

Borovsky, J. E., B. Lavraud, and M. M. Kuznetsova (2009), Polar cap potential saturation, dayside reconnection, and changes to the magnetosphere, *J. Geophys. Res.*, *114*, A03224, doi:10.1029/2009JA014058.

Clauer, C. R., R. L. McPherron, C. Searls, and M. G. Kivelson (1981), Solar wind control of auroral zone geomagnetic activity, *Geophys. Res. Lett*, *8*(8), 915–918, doi:10.1029/GL008i008p00915.

Clauer, C. R., Z. Xu, M. Maimaiti, J. M. Ruohoniemi, W. Scales, M. D. Hartinger, M. J. Nicolls, S. Kaeppler, F. D. Wilder, and R. E. Lopez (2016), Investigation of a rare event where the polar ionospheric reverse convection potential does not saturate during a period of extreme northward IMF solar wind driving, *J. Geophys. Res. Space Physics*, *121*, 5422–5435, doi:10.1002/2016JA022557.

Hill, T. W., A. J. Dessler, and R. A. Wolf (1976), Mercury and Mars: The role of ionospheric conductivity in the acceleration of magnetospheric particles, *Geophys. Res. Lett.*, *3*(8), 429–432.

Ilie, R., M. W. Liemohn, and A. Ridley (2010), The effect of smoothed solar wind inputs on global modeling results, *J. Geophys. Res.*, *115*, A01213, doi:10.1029/2009JA014443.

Kan, J. R., and L. C. Lee (1979), Energy coupling function and solar wind-magnetosphere dynamo, *Geophys. Res. Lett.*, *6*, 577–580, doi:10.1029/GL006i007p00577.

Kilpua, E. K. J., A. Isavnin, A. Vourlidas, H. E. J. Koskinen, and L. Rodriguez (2013), On the relationship between interplanetary coronal mass ejections and magnetic clouds, *Ann. Geophys.*, *31*(7), 1251–1265.

Kivelson, M. G., and A. J. Ridley (2008), Saturation of the polar cap potential: Inference from Alfvén wing arguments, *J. Geophys. Res.*, *113*, A05214, doi:10.1029/2007JA012302.

Lavraud, B., and J. E. Borovsky (2008), Altered solar wind-magnetosphere interaction at low Mach numbers: Coronal mass ejections, *J. Geophys. Res.*, *113*, A00B08, doi:10.1029/2008JA013192.

Lopez, R. E., R. Bruntz, E. J. Mitchell, M. Wiltberger, J. G. Lyon, and V. G. Merkin (2010), Role of magnetosheath force balance in regulating the dayside reconnection potential, *J. Geophys. Res.*, *115*, A12216, doi:10.1029/2009JA014597.

Myllys, M., E. Kilpua, B. Lavraud, and T. Pulkkinen (2006), Solar wind-magnetosphere coupling efficiency during ejecta and sheath driven geomagnetic storms, *J. Geophys. Res.*, *121*, 4378–4396, doi:10.1002/2016JA022407.

Ober, D. M., N. C. Maynard, and W. J. Burke (2003), Testing the Hill model of transpolar potential saturation, *J. Geophys. Res.*, *108*(A12), 1467, doi:10.1029/2003JA010154.

Pulkkinen, T. I., A. P. Dimmock, A. Osmane, and K. Nykyri (2015), Solar wind energy input to the magnetosheath and at the magnetopause, *Geophys. Res. Lett.*, *42*, 4723–4730, doi:10.1002/2015GL064226.

Pulkkinen, T. I., A. P. Dimmock, A. Lakka, A. Osmane, E. Kilpua, M. Myllys, E. I. Tanskanen, and A. Viljanen (2016), Magnetosheath control of solar wind-magnetosphere coupling efficiency, *J. Geophys. Res. Space Physics*, *121*, 8728–8739, doi:10.1002/2016JA023011.

Raeder, J., and G. Lu (2005), Polar cap potential saturation during large geomagnetic storms, *Adv. Space Res.*, *36*(10), 1804–1808.

Reiff, P. H., and J. G. Luhmann (1986), Solar wind control of the polar-cap voltage, in *In Solar Wind Magnetosphere Coupling*, vol. 126, edited by Y. Kamide and J. A. Slavin, pp. 453–476, Terra Sci., Tokyo.

Reiff, P. H., R. W. Spiro, and T. W. Hill (1981), Dependence of polar cap potential drop on interplanetary parameters, *J. Geophys. Res.*, *86*(A9), 7639–7648.

Ridley, A. J. (2005), A new formulation for the ionospheric cross polar cap potential including saturation effects, *Ann. Geophys.*, *23*(11), 3533–3547.

Ridley, A. J. (2007), Alfven wings at Earth's magnetosphere under strong interplanetary magnetic fields, *Ann. Geophys.*, *25*(2), 533–542. Copernicus GmbH.

Ridley, A. J., and E. A. Kihn (2004), Polar cap index comparisons with AMIE cross polar cap potential, electric field, and polar cap area, *Geophys. Res. Lett.*, *31*, L07801, doi:10.1029/2003GL019113.

Russell, C. T., J. G. Luhmann, and G. Lu (2001), Nonlinear response of the polar ionosphere to large values of the interplanetary electric field, *J. Geophys. Res.*, *106*(A9), 18,495–18,504.

Shepherd, S. G. (2007), Polar cap potential saturation: Observations, theory, and modeling, *J. Atmos. Sol. Terr. Phys.*, *69*(3), 234–248.

Siscoe, G. L., G. M. Erickson, B. U. Ö. Sonnerup, N. C. Maynard, J. A. Schoendorf, K. D. Siebert, D. R. Weimer, W. W. White, and G. R. Wilson (2002a), Hill model of transpolar potential saturation: Comparisons with MHD simulations, *J. Geophys. Res.*, *107*(A6), 1075, doi:10.1029/2001JA000109.

Siscoe, G. L., N. U. Crooker, and K. D. Siebert (2002b), Transpolar potential saturation: Roles of region 1 current system and solar wind ram pressure, *J. Geophys. Res.*, *107*(A10), 1321, doi:10.1029/2001JA009176.

Takalo, J., K. Mursula, and J. Timonen (2000), Role of the driver in the dynamics of a coupled-map model of the magnetotail—Does the magnetosphere act as a low-pass filter?, *J. Geophys. Res.*, *105*(A12), 27,665–27,672, doi:10.1029/2000JA900114.

Troshichev, O., H. Hayakawa, A. Matsuoka, T. Mukai, and K. Tsuruda (1996), Cross polar cap diameter and voltage as a function of PC index and interplanetary quantities, *J. Geophys. Res.*, *101*(A6), 13,429–13,435.

Vasyliunas, V. M., J. R. Kan, G. L. Siscoe, and S. I. Akasofu (1982), Scaling relations governing magnetospheric energy transfer, *Planet. Space Sci*, *30*(4), 359–365.

Weimer, D. R., L. A. Reinleitner, J. R. Kan, L. Zhu, and S. I. Akasofu (1990), Saturation of the auroral electrojet current and the polar cap potential, *J. Geophys. Res.*, *95*(A11), 18,981–18,987.

Wilder, F. D., C. R. Clauer, J. B. H. Baker, E. P. Cousins, and M. R. Hairston (2011), The nonlinear response of the polar cap potential under southward IMF: A statistical view, *J. Geophys. Res.*, *116*, A12229, doi:10.1029/2011JA016924.

Wilder, F. D., S. Eriksson, and M. Wiltberger (2015), The role of magnetic flux tube deformation and magnetosheath plasma beta in the saturation of the Region 1 field-aligned current system, *J. Geophys. Res. Space Physics*, *120*, 2036–2051, doi:10.1002/2014JA020533.